Inorganic Chemistry

Article

pubs.acs.org/IC

Generalized Approach to the Microstructure Direction in Metal Oxide Ceramics via Polymerization-Induced Phase Separation

Stephen G. Rudisill,[†] Sammy Shaker,[†] Denis Terzic,[†] Réginald Le Maire,[‡] Bao-Lian Su,[‡] and Andreas Stein*[,†]

[†]Department of Chemistry, University of Minnesota, 207 Pleasant St. SE, Minneapolis, Minnesota 55455, United States

[‡]Laboratory of Inorganic Materials Chemistry, University of Namur, Rue de Bruxelles 61, B-5000 Namur, Belgium

Supporting Information

ABSTRACT: When three-dimensionally ordered macroporous (3DOM) materials are synthesized in polymeric colloidal crystal templates using a Pechini-type approach, polymerization-induced phase separation (PIPS) can occur. Depending on the reaction conditions, the porous products have a variety of morphologies, including an extended inverse opal structure, bicontinuous networks of 3DOM materials interrupted by extended voids, uniform 3DOM microspheres, sheet structures of templated macroporous oxides, and hollow particles obtained by structural disassembly. In this study, the mechanism underpinning morphology control of 3DOM metal oxides through PIPS is elucidated for $Ce_{0.5}Mg_{0.5}O_{1.5}$ and CeO_2 systems. The mechanistic information is then applied to synthesize target morphologies for Mn_3O_4 and Fe_2O_3/Fe_3O_4 systems, demonstrating the more general nature of the synthetic approach for aqueous metal precursors that can be complexed with citric acid. The effects of reactant balance, complexation behavior, processing temperature, and template sphere size are related directly to the microstructures obtained. The predominant controlling factor of microstructural evolution in PIPS Pechini precursors is found to be the degree of polymerization of the polyester, which can be controlled through tailoring the reagent imbalance. 3DOM microspheres produced by the method are between 0.5 and 3 μm in size, with polydispersities below 25%.

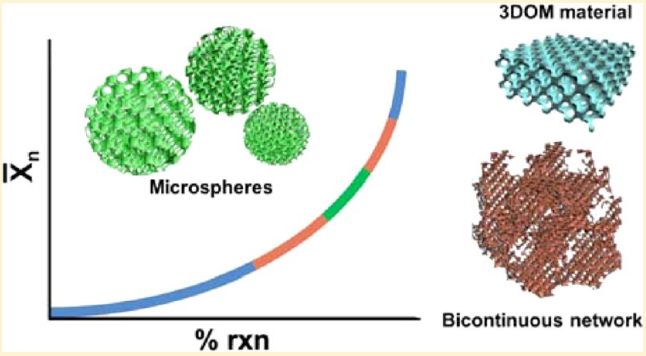

INTRODUCTION

Porous metal oxides are of great importance to a variety of chemical processes and technologies. In particular, hierarchical structures incorporating both micrometer-scale and nanoscale features allow for increased surface area while maintaining open access to that surface area via a controlled microstructure.[1] This is an advantage in applications such as heterogeneous catalysis,[2−4] and fuel cells,[5−8] where mass transfer and chemically accessible surface area dominate efficiency.[9] Additionally, spatial isolation of ceramic structural features through the introduction of void space has been shown to reduce the sintering behavior in high-temperature reactions.[10] The chromatography column efficiency can be improved by incorporating microstructured matrices.[11] Considering the above examples, the discovery, exploration, and optimization of chemical routes to porous ceramic particles with defined internal and external shapes and sizes are of interest to many different technical fields.

The sol−gel method is often used to synthesize metal oxide ceramics, owing to its versatility and relative ease of synthesis.[12−14] Within this general scheme of preparing a solution, condensing it into a gel, and calcining to obtain the final product, structure-modifying techniques such as hard[15,16] and soft templating[17−19] can be employed to create porosity on differing length scales. In addition to incorporating internal pore structure via hard templating, it is sometimes possible to control the external shape of the porous products at the micrometer scale. For example, shaped CuO particles possessing a network of ordered pores have been synthesized by electrodeposition inside a colloidal crystal template (CCT) by modifying the deposition conditions and electrolyte choice.[20] Sheets and other microstructures have been introduced to electrodeposited macroporous ZnO by modifying the colloidal crystal surface chemistry or adding surfactants.[21] Other three-dimensionally ordered macroporous (3DOM) particles have been generated by growing single crystals within a CCT,[22] with the resultant particle shapes determined by the crystal shape.[23]

A convenient method of generating micrometer-scale structures within sol−gel precursors is polymerization-induced phase separation (PIPS). Originally discovered in sol−gel syntheses of silica using silicon alkoxides,[24] PIPS occurs as a result of the growing dissimilarities (polarity, electrostatics, and

Special Issue: To Honor the Memory of Prof. John D. Corbett

Received: September 29, 2014
Published: November 14, 2014

   dx.doi.org/10.1021/ic5023856 | Inorg. Chem. 2015, 54, 993−1002

viscosity) between a polymerizing silica gel and its solvent. These dissimilarities cause a gradual phase separation of the silica oligomers, which produces micrometer-scale solvent-rich and silica-rich regions within the precursor. By tailoring the reaction rate and equilibrium state[25] of the silica formation process, microstructures present at different points during the gelation of the precursor can be "locked in" and realized in the final structure obtained after calcination. The target structures can be modified in shape and size by changing the gelation temperatures and reaction times, as well as the choice of reagents and their molar ratios. Changing the silicon alkoxide concentration, adding methanol or ethanol to the aqueous solvent to modify its polarity,[25] increasing the acidity of the solvent,[25] and adding hydrophilic polymers to the system[26,27] all have substantial effects on the resulting microstructure.

Recently, we demonstrated that morphologies very similar to those observed in these silica systems could be obtained in Pechini-type syntheses of 3DOM $Ce_{0.5}Sr_{0.5}O_{1.5}$, $Ce_{0.5}Mg_{0.5}O_{1.5}$, and CeO_2.[28] The Pechini method[29] is a sol−gel technique for forming metal oxide ceramics with small crystallite sizes and (in the case of solid solutions) homogeneity. It involves the formation of a metal−carboxylic acid complex, typically with citric acid (CA), and then a polymerization of those complexes with a polyol such as ethylene glycol (EG) to form a metal-laced polyester. The primary advantage of this method is that the metal cations, bound to the polymer, remain isolated from each other and do not aggregate or produce crystalline products prior to the burnout of the polyester. This leads to the smaller, homogeneous crystallites mentioned above.

In our prior publication, we demonstrated that these chelate-controlled sol−gel reactions carried out in the confinement of a CCT yield materials whose morphologies are, in part, controlled by interactions with the template but on a length scale beyond that of individual colloids in the template.[28] In particular, using examples of solid solutions based on cerium oxide, we demonstrated the formation of uniform macroporous microspheres or bicontinuous structures with hierarchical porosity. In the microspheres, the macropores were molded by the CCT, but the external spherical shape was derived from confined nucleation and growth during step-growth polymerization of the precursor gel. The hierarchically structured materials, on the other hand, resulted from spinodal decomposition of the gel phases within the CCT. However, several open questions remained relating to the effect of the extent of polymerization of the metal-laced polyester on the microstructure, the role of the cations in the generation of the microstructure, and the applicability of the technique to non-cerium-based metal oxides.

The present study addresses these open questions and deepens our understanding of PIPS in templated Pechini gels. We employ a number of synthetic strategies and modifications for cerium-based systems to probe the effects of electrostatics, gel molecular weight, cation charge and oxidation state, and precursor−template interactions on PIPS-induced morphology. In addition, we demonstrate the wider applicability of morphology control by PIPS in CCTs with two test cases: Fe_2O_3 and Mn_3O_4 systems.

EXPERIMENTAL SECTION

Template Synthesis. CCTs were synthesized through emulsifier-free emulsion polymerization of methyl methacrylate to produce colloidal poly(methyl methacrylate) (PMMA) spheres, followed by gravity sedimentation of those spheres into face-centered-cubic (fcc) arrays.[30] KPS was used as an initiator. The diameters of the PMMA spheres were varied by adjusting the amount of KPS and the amount of water in the synthesis. Three sets of spheres were obtained, with the following diameters and standard deviations: 362 ± 3, 395 ± 3, and 489 ± 4 nm. The polymerization produced aqueous colloidal dispersions containing ca. 20 wt % PMMA, which were then poured into crystallization dishes, covered with aluminum foil, and sedimented to form the CCTs.

Synthesis of Porous Microspheres and Bicontinuous Networks. Precursors were prepared by dissolving a metal nitrate salt (M^{q+}), CA, and EG in water. The metal nitrates used were $Fe(NO_3)_3\cdot 9H_2O$, $Mn(NO_3)_2\cdot 4H_2O$, $Ce(NO_3)_3\cdot 6H_2O$, and/or $Mg(NO_3)_2\cdot 6H_2O$. For one experiment, $Ce(NO_3)_3\cdot 6H_2O$ was replaced with $CeCl_3\cdot 7H_2O$. The water/total metal ion (TMI) molar ratio was kept constant at 36:1. The molar ratios of EG/CA/TMI in the precursor were varied to produce different samples, which are designated by these ratios in the form M_xO_y XYZ. Some samples were produced by substituting malic acid for CA and glycerin for EG.

The precursor solutions were infiltrated in CCTs and heat-treated at 90 °C for 24 h in tightly sealed glass vials, causing the precursor to form a hard gel within the template. Different gelation temperatures were used for some samples to investigate the morphological effects. Once gelled, the samples were calcined in a tube furnace under static air at 310 and 450 °C (2 °C/min ramp; 2 h dwell time at each temperature).

RESULTS AND DISCUSSION

Overview of the Structures and Morphologies Observed. Scanning electron microscopy (SEM) images of the materials synthesized by combining the Pechini method with colloidal crystal templating reveal a variety of microstructural features. These features can be grouped into a series of categories, including microspheres, spheroids, bicontinuous materials, dense networks, and lamellar structures (Table S1 in the Supporting Information, SI). Materials defined as "microspheres" contain spherical objects with macropores derived from the PMMA template. Depending on the precursor composition, spheres may have different sizes and may interconnect. In a few compositions, the distinct objects are not regularly spherical and are then denoted as "spheroids". The microsphere morphology is the primary target of this investigation for two reasons. First, the microspheres are comparatively easier to characterize in shape and size, allowing for more quantitative comparisons between differing precursor and metal oxide compositions. Second, the number of precursor compositions that produce microspheres is limited, indicating a degree of precision required to control the sample morphology.

"Bicontinuous network" refers to structures in which two interpenetrating phases are present (i.e., 3DOM material with templated pores and void spaces not defined by the hard template), where the two phases appear to be fully interconnected. The bicontinuous networks come in two varieties, "wormlike" and "chunks", depending on the structure of the 3DOM material. The terms "open" and "dense" are used to qualitatively describe the ratio of porous solid to void space that is not templated by the CCT, with "open" structures having more void space and "dense" structures having more solid material. Bicontinuous networks are typically observed with precursor compositions that deviate slightly from those that produce microspheres. Bicontinuous networks are the secondary target of this investigation because they represent a class of structures with hierarchical porosity. A large number of compositions produce structures of this type, but because of the nonuniform nature of the network morphology and the

dx.doi.org/10.1021/ic5023856 | Inorg. Chem. 2015, 54, 993−1002

differing ratios of porous solid to untemplated void space, it is more difficult to measure the features of these structures and make meaningful quantitative comparisons between samples.

"Dense network" refers to structures that are mostly filled with porous solid and do not contain additional precursor-induced microstructural variation. These are the typical 3DOM structures or inverse opal structures that are normally targeted by colloidal crystal templating methods. However, some of these dense networks contain micrometer-scale holes that are not continuous; these holes likely arise from precursor effects (PIPS) rather than incomplete infiltration of the CCT. In addition, some unique structures are obtained in narrow regions of quasi-phase space, including a lamellar structure, but the categories of microspheres, bicontinuous networks, and dense networks serve to describe the vast majority of structures observed in this work. "Hollow spheres" refer to structures composed of spherical thin shells of metal oxide with a narrow, strongly bimodal distribution of sizes. The diameters of these spheres are substantially smaller in this study than those of the original CCT spheres.

Previously we observed morphological variations arising from Pechini method syntheses of CeO_2 and the mixed oxide $Ce_{0.5}Mg_{0.5}O_{1.5}$ using CA as a complexing agent and EG as a cross-linker.[28] These metal oxide compositions have a relatively large region in quasi-phase space that yields microspheres and spheroids of different sizes. Given the wide space available for the generation of microspheres and bicontinuous networks with these compositions, we examined the effects of a variety of reagent substitutions on the microstructures in greater detail.

Molecular Weight, Stoichiometric Balance, and Morphology. Pechini gels are step-growth polyesters formed by a condensation reaction between EG and CA. The relationship between the extent of reaction during gelation processes and the relative ratio of monomers has been described in detail in the literature on step polymerization.[31] Specifically, the degree of polymerization $\bar{X}_n$ (the number-average value of monomer units present in the products of a polymerization reaction) is given by Carothers equation $\bar{X}_n = 2/(2 - pf_{avg})$ for stoichiometric amounts of reactants, where p is the extent of the reaction, $f_{avg} = \sum N_i f_i / \sum N_i$, and N_i is the number of molecules of monomer i with functionality f_i. For nonstoichiometric reaction mixtures, the relationship becomes more complex because the extent of polymerization is limited by the deficient reactant, and the excess reagent lowers the functionality of the system.

To demonstrate the relationship of the degree of polymerization, and thus molecular weight, to the microstructure observed, a series of samples were produced using different conditions but the same molar ratios in the precursor. These compositions, $Ce_{0.5}Mg_{0.5}O_{1.5}$ 211 and CeO_2 132, were selected because they are known to produce microspheres of moderate size, allowing facile detection of structural changes both small (e.g., microsphere diameter) and large (e.g., formation of bicontinuous networks).

The condensation reaction to form the preceramic metal-laced polyesters is activated by heat. A simple experiment to observe the dependence of the structure on the molecular weight is to see how the structure changes with different gelation temperatures (Figure 1). The degree of polymerization is proportional to the polymerization rate constant (itself a temperature-dependent value),[32] and so a slight reduction in the gel temperature from 90 to 80 °C and a shortened gelation time results in a substantial reduction in the sphere size, from

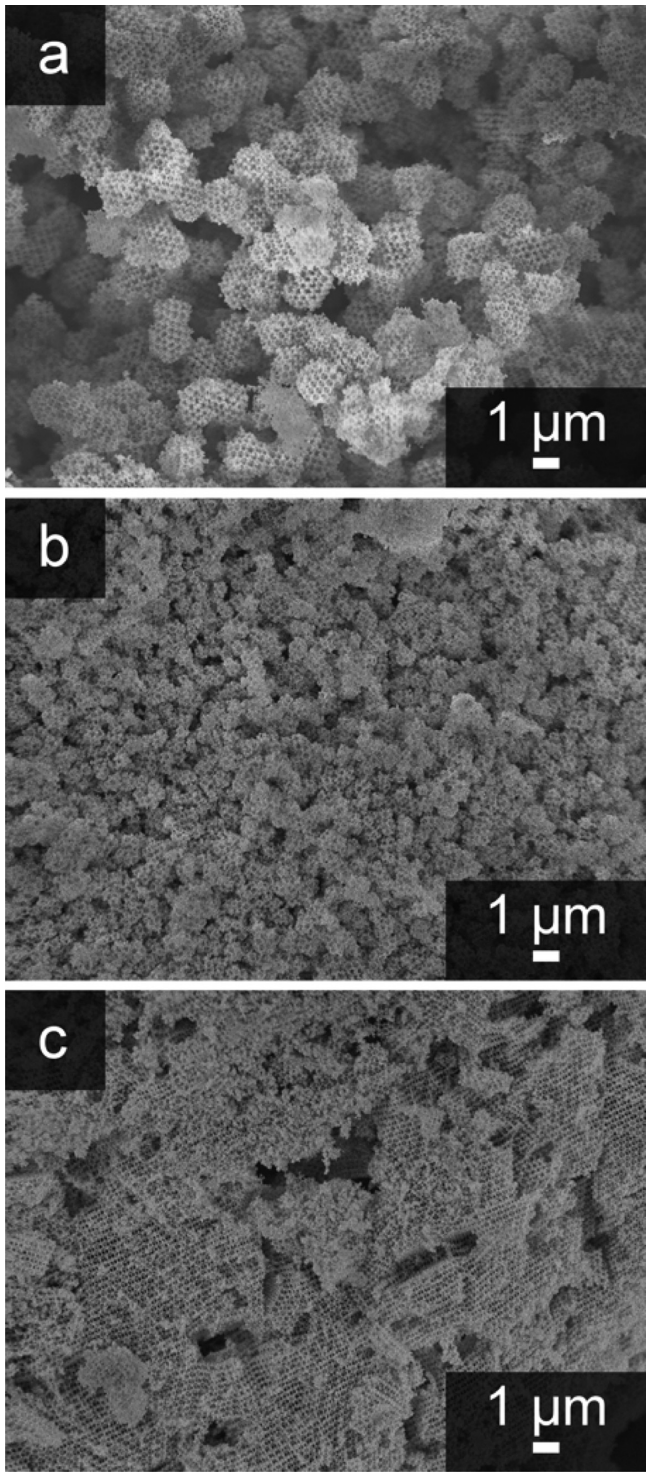

Figure 1. SEM micrographs of CeO_2 132 treated at (a) 90 °C for 24 h, (b) 80 °C for 16 h, and (c) 40 °C for 24 h. These samples were prepared using 489 nm PMMA spheres in the CCT and a nitrate precursor.

1.60 ± 0.11 to 0.58 ± 0.08 μm (Figure 1b). Meanwhile, greater reductions in the temperature result in a loss of the sphere morphology and the production of a more monolithic 3DOM structure with isolated void spaces (Figure 1c).

The final molecular weight distribution obtained depends on the balance of monomer "end groups", in this case the balance of carboxylate to hydroxyl moieties. To modify the molecular

dx.doi.org/10.1021/ic5023856 | Inorg. Chem. 2015, 54, 993−1002

weight of the gel without substantially changing the molar ratios of organic components to metal to water, CA and EG can be substituted with other poly(carboxylic acid)s and polyols. In this study, we used the $Ce_{0.5}Mg_{0.5}O_{1.5}$ 211 precursor composition but substituted CA for malic acid and EG for glycerin (Figure S2 in the SI) in order to modify the number of reactive groups available for esterification without changing the organic, metal ion, and water molar ratios. This demonstrated drastic changes in the morphology as they relate to functional group balance, indicating that the degree of polymerization controls not only the microsphere size but also the morphology of the material.

Clear morphological variations result from substitutions of these reagents (Figure 2). With glycerin replacing EG, the

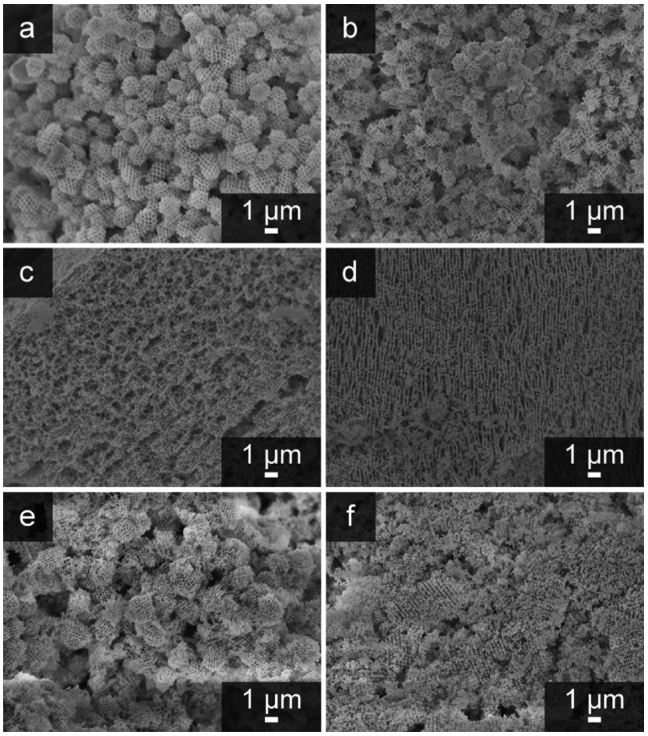

Figure 2. SEM micrographs of $Ce_{0.5}Mg_{0.5}O_{1.5}$ 211 sample preparations with (a) no reagent substitutions, (b) substitution of glycerin for EG, (c) substitution of malic acid for CA, and (d) substitution of both glycerin and malic acid for EG and CA, respectively. All of the above samples were prepared using 489 nm PMMA spheres in the CCT. (e) $Ce_{0.5}Mg_{0.5}O_{1.5}$ 211 prepared with 395 nm PMMA spheres and no reagent substitutions. (f) $Ce_{0.5}Mg_{0.5}O_{1.5}$ 211 prepared with 362 nm PMMA spheres and no reagent substitutions. All samples were prepared from nitrate metal salts and were gelled at 90 °C for 24 h.

spheres produced from the otherwise unmodified synthesis are smaller in diameter. Whereas the original spheres have a mean size of 1.32 ± 0.16 μm (Figure 2a), the glycerin-modified synthesis produces spheres with a mean size of 0.91 ± 0.17 μm (Figure 2b). Glycerin supplies one more −OH group per mole than EG, which affects the reactant balance. Considering that the EG component is already in excess of the CA monomer for the 211 composition, it is expected that a further increase in the number of −OH groups would limit the extent of polymerization. This confirms our previous conclusion that the reactant/functional group balance (i.e., gel molecular weight) is responsible for sphere size control. Additionally, the walls of the structure have been substantially coarsened, which is the result of excess glycerin partially swelling the PMMA template spheres and thus distorting the wall structure (Figure S3 in the SI). The malic acid substituted synthesis does not generate spheres at all; rather, it produces a bicontinuous network that has not been observed for the $Ce_{0.5}Mg_{0.5}O_{1.5}$ 211 composition.

The above results link a series of factors that influence the average degree of polymerization (i.e., number-average chain length) to the microstructural morphology obtained. In the course of this work, numerous other samples with varied precursor composition (Table S1 in the SI) were prepared. On the basis of the morphologies observed for all of these samples, we propose that the microstructures follow a continuum determined by the reaction extent/molecular weight of the Pechini polyester (Figure 3). When the extent of reaction is low (e.g., with a high reactant imbalance), the precursor is a solution consisting of relatively soluble oligomers that can pass freely throughout the interstitial space between spheres in the CCT. These oligomers fill that space evenly, and minimal microstructural effects from PIPS are observed. As the average molecular weight of the polyester increases, these oligomers combine to form longer-chain polymers in the void space, creating polymer-rich regions in the aqueous solution. As the molecular weight of the polymer increases further along with the difference in polarity between the solvent-rich and polymer-rich regions, the polymer-rich regions tend to minimize their interfacial area with the solvent, forming microspheres. For systems with less reactant imbalance, the polymerization process continues to progress and the spheres combine, forming a denser microstructure network in which void spaces are interconnected but smaller. Finally, at the highest extent of reaction, the gel fully densifies into large "blocks" greater than 50 μm diameter. The only micrometer-scale void spaces in the structure are cracks between these blocks that develop during drying and calcination of the infiltrated template.

Further investigation of the involvement of the template, particularly with regard to confinement of the growing polyester gel within the PMMA CCT, has generated additional insight. With a decrease in the diameter of the template spheres, two properties of the template−precursor interaction are affected: molecular motion/diffusion of the polymer precursor and template−precursor interfacial area. As the PMMA sphere diameter decreases, the size of the void space between templating spheres—specifically the octahedral and tetrahedral holes in the fcc array—concurrently decreases. This may lead to "pinning" of polymer molecules once they reach a given molecular weight, preventing the expected phase separation behavior from occurring. Likewise, as the sphere diameter decreases, the specific surface area of the template increases. The presence of intermolecular forces between the precursor and template (electrostatics and hydrogen bonding) was demonstrated to have an effect on the morphology in previous work.[28]

The effect of the sphere size on the phase separation behavior was studied by synthesizing the $Ce_{0.5}Mg_{0.5}O_{1.5}$ 211 composition inside the CCTs with sphere diameters of 362, 395, and 489 nm. With 489 nm spheres, the 211 precursor composition produces uniform 3DOM microspheres (Figure 2a). SEM images reveal deviations from this microsphere morphology when smaller templating spheres are employed. With 395 nm templates, some microspheres are present, but the morphology is less consistent, and some areas of the sample (Figure 2e, left side of the image) are more reminiscent of the bicontinuous networks. The spheres that are present are

dx.doi.org/10.1021/ic5023856 | Inorg. Chem. 2015, 54, 993−1002

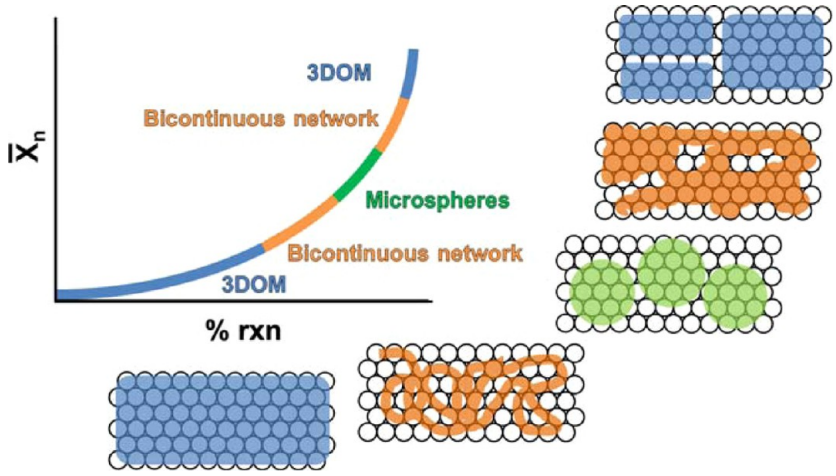

Figure 3. Correlation of the observed structures to a typical step-growth polymerization plot of the degree of polymerization ($\bar{X}_n$) versus the extent of reaction (% rxn), that is, the polyesterification reaction between CA complexes with EG. "3DOM" refers to an extended macroporous structure that is defined only by the CCT with no discernible microstructure aside from the ordered network of pores left after template removal.

larger—1.95 ± 0.27 μm, compared with 1.32 ± 0.16 μm for the 489 nm template—and partially merged with one another. For 362 nm templates, the sphere morphology is absent, and domains have merged together more extensively (Figure 2f). The decreased diffusion capability of the polyesters in a matrix with narrower void spaces creates an additional constraint on the ability of the growing polymers to collide, resulting in a lower molecular weight and thus a different morphology.

Obstacles to Generalization. Extending the PIPS methodology via the Pechini method to other metal oxide systems seems trivial at first glance. Tuning the reagent imbalance between CA and EG offers a powerful and direct route to manipulating the molecular weight of the Pechini polymers. However, examining the system from this perspective leads one to overlook the more crucial "reagent" balance, i.e., the balance between EG and CA *complexes* of metal ions. Different metal ions have different formation constants (K_f) for CA complexes, leading to different stoichiometries in solution than the apparent EG/CA ratio. In fact, this behavior can be directly observed in the CeO_2 system because the formation of CeO_2 from the reagents used in this study requires a change in the oxidation state.

$Ce(NO_3)_3{\cdot}6H_2O$ is used as the cerium source for most of our experiments. However, replacing the NO_3^- counterions with Cl^- results in a complete change in the morphology for an otherwise identical precursor composition (Figure 4a,b). This occurs because the NO_3^- ions participate in a redox reaction during the gelation step, namely, the oxidation of Ce^{3+} to Ce^{4+}. When the oxidizing NO_3^- ions are replaced with the weakly reducing Cl^-, this oxidation does not occur during the gelation step, as evidenced by the lack of a color change (Figure 4d) upon removal from the oven. Ce^{3+} ions are colorless, whereas Ce^{4+} ions are yellow, thus the coloration of the resultant powders after calcination. This change in the oxidation state would be accompanied by a change in K_f for the CA/Ce^{q+} complex, resulting in the altered morphology.

When the concentration of NO_3^- in a $Ce_{0.5}Mg_{0.5}O_{1.5}$ precursor is doubled by adding HNO_3 to the solution, spheres are still formed, but they are larger and have, in fact, partially collided to form a bulbous bicontinuous network structure (Figure 4c). An equal number of protons have been added, but because the nitrate precursor solutions are at or below pH 1

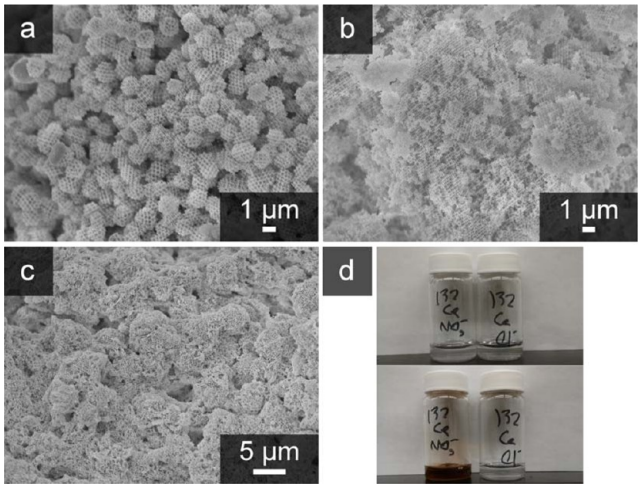

Figure 4. SEM images and photographs depicting the influence of counterions in metal precursors on the microstructure. (a) SEM image of $Ce_{0.5}Mg_{0.5}O_{1.5}$ 211 prepared with $Ce(NO_3)_3{\cdot}6H_2O$, reproduced from Figure 2a for comparison. (b) SEM image of $Ce_{0.5}Mg_{0.5}O_{1.5}$ 211 prepared with $CeCl_3{\cdot}7H_2O$. (c) SEM image of $Ce_{0.5}Mg_{0.5}O_{1.5}$ 211 with doubled NO_3^- concentration. (d) Photographs of CeO_2 132 precursor solutions before (top) and after gelation at 90 °C for 18 h (bottom). The gelation time was 24 h for the samples depicted in parts a–c. All samples were prepared using 489 nm spheres in the CCT.

upon formation, the effect on the pH is limited. We propose that this behavior is a result of enhanced charge screening due to an increase in the concentration of NO_3^-, resulting in a lower Debye length for the growing polyesters.

Another aspect of the CA/Ce^{q+} interaction that must be kept in mind is that the binding strength and binding environment of the cation may be altered by a change in the oxidation state. A stronger chelation of Ce^{4+} may result in reduced lability of the carboxylic acid groups of CA, which have a dual function as the binding agents for cerium cations as well as the end groups for the polyesterification reaction.[33] If carboxylic acid groups become unavailable for condensation, the reactant balance will be modified, resulting in unintended changes in the molecular weight (and, thus, morphology). This will be discussed further in the exploration of Fe_2O_3 and Mn_3O_4 systems as test cases for

dx.doi.org/10.1021/ic5023856 | Inorg. Chem. 2015, 54, 993–1002

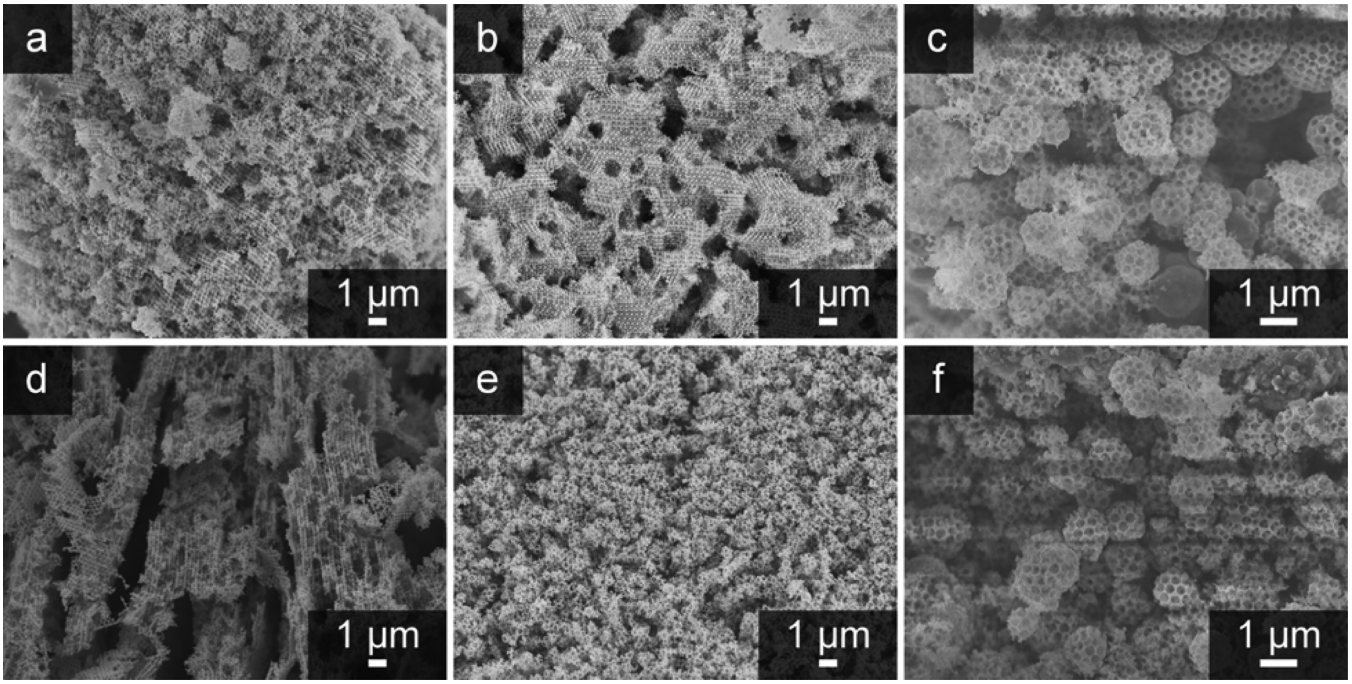

Figure 5. SEM images of Mn_3O_4 and Fe_2O_3 compositions: (a) Mn_3O_4 132; (b) Mn_3O_4 331; (c) Mn_3O_4 341; (d) Fe_2O_3 111; (e) Fe_2O_3 615; (f) Fe_2O_3 113. All samples were prepared using 489 nm spheres in the CCT and were gelled at 90 °C for 24 h.

the general applicability of PIPS-based microstructural control in hard templates.

Morphological Variation in Fe_2O_3 and Mn_3O_4 Pechini Gels. Fe_2O_3 and Mn_3O_4 were selected as test systems based on their interactions with CA. We chose systems that had binding modes similar to those observed in the lanthanides but presented substantial shifts in K_f and the oxidation state of the final products. Mn^{2+} and Fe^{3+} serve these purposes appropriately for the available data. The phases of the oxides were confirmed by X-ray diffraction (XRD; Figure S4 in the SI). The iron oxide samples contained some magnetite, Fe_3O_4, as an impurity phase, but the samples will be referred to here by the majority phase, Fe_2O_3.

As expected, varying the precursor composition drastically affects the observed morphology in the sample (Figure 5). The Mn_3O_4 132 and Fe_2O_3 111 compositions (Figure 5a,d) correspond to EG/CA/M^{q+} ratios, which produced microspheres for CeO_2 and $Ce_{0.5}Mg_{0.5}O_{1.5}$, respectively, clearly demonstrating that the change in the cation identity and charge changed the phase separation behavior of the precursor gel. Bicontinuous networks are obtained for a variety of compositions in both systems; an example is shown in Figure 5b. Fe_2O_3 615 (Figure 5e) consists of microspheres where the diameter only encompasses 4−5 pores, making it difficult to discern edges and accurately measure the dispersion. More discernible microspheres are obtained for the compositions Mn_3O_4 341 and Fe_2O_3 113 (Figure 5c,f). Finally, a unique lamellar structure was observed for Fe_2O_3 313 (Figure S8g in the SI).

The Mn_3O_4 spheres are 1.30 ± 0.3 μm in diameter, and the Fe_2O_3 spheres are 1.32 ± 0.29 μm, with coefficients of variation (c_v and $\bar{x}/\sigma$) of 23% and 22%, respectively. These spheres are less uniform than the $Ce_{0.5}Mg_{0.5}O_{1.5}$ microspheres obtained in previous work (c_v = 15%) but similar to those prepared in the syntheses of phase-pure CeO_2 microspheres (c_v = 20%).[28]

These samples reveal a strong correlation between K_f for CA, the molar ratio of CA to metal cation, and the ultimate morphology of the sample. The selected cation has a pronounced effect on the reagant balance in the polyesterification due to differences in CA complex formation, underlining the critical importance of compensating for this behavior when applying the method of template-confined PIPS to different metal oxides. The results further confirm that the reagent balance (molecular weight) is the primary determinant of the morphology obtained by this method and thus provide a semiempirical rule of thumb for generalization. Essentially, in order to "translate" a target microstructure—here, the microsphere morphology is considered the target because it is recognizable and easy to characterize—from one metal oxide to another, one must compensate for K_f of the metal by adjusting the CA concentration in the correct direction (Table 1) via Le

Table 1. K_f Data and Binding Modes for Ce^{3+}, Mn^{2+}, and Fe^{3+}

cation	binding mode[34]	K_f (CA)[34]	microsphere CA/M^{q+}
Mn^{2+}	Mn(Cit)	4.15	4:1
Ce^{3+}	Ce(Cit)	7.95	1.5:1
Fe^{3+}	Fe(Cit)	11.5	1:3

Chatelier's principle. For lower K_f, this means driving the formation reaction with excess CA, whereas for higher K_f, this means limiting the formation of complex by reducing the CA concentration. Mn^{2+} and Fe^{3+} are good "brackets" for this investigation because most cations of interest have a CA K_f falling somewhere between 4 and 11.5.

Tuning the Templating Behavior via Precursor Composition. Several studies of precursor−template interactions in 3DOM materials have focused on how the opal structure of the template is replicated in the templated product.[35−38] Common structures observed in CCT-templated

dx.doi.org/10.1021/ic5023856 | Inorg. Chem. 2015, 54, 993−1002

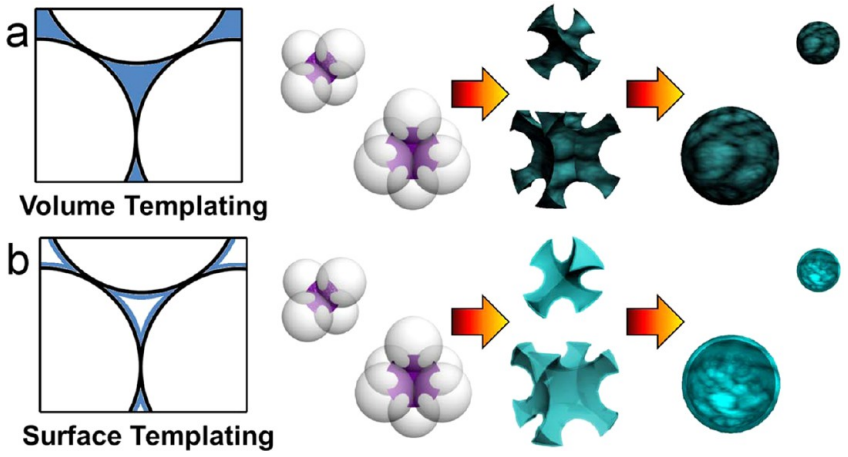

Figure 6. Graphical depiction of the metal oxide particle morphology obtained in the CCT in the two types of templating processes: (a) volume templating, where complete filling of the void spaces between spheres occurs; (b) surface templating, where metal ions or metal-containing precursors preferentially fill interstices at the sphere surfaces, leaving solvent or combustible material in the center of the voids. Volume templating combined with the particle disassembly of a 3DOM structure results in solid particles produced from the original tetrahedral and octahedral template voids.[39,40] Surface templating produces hollow particles in a similar manner.

materials are negative replicas of the CCT, or "volume-templated" materials, in which the void space between spheres is completely filled by the ceramic material in the final product (Figure 6a). Other structures in which the majority of the solid material forms at the surface of the template spheres ("surface-templated" materials) are formed in systems with strong precursor−template interactions and can produce hollow shapes in the interstitial region of the CCT and, in some cases, discrete hollow spheres around the original template spheres (Figure 6b).

We have observed hollow structures in 3DOM Mn_3O_4, for which under EG-rich conditions (Mn_3O_4 411, 611, and 711) and a small CCT sphere diameter (362 nm) a bimodal distribution of hollow spheres is obtained (Figure 7a). However, the spheres are too small (∼100 and ∼40 nm) to be simply replicas of the templating spheres. These sizes correlate reasonably well with the octahedral and tetrahedral holes of the template, allowing for shrinkage that is typically observed after calcination; for a 362 nm CCT, these holes are approximately 150 and 81 nm, respectively (see the SI).

We propose that these morphologies are also accessible through precursor design in Pechini PIPS systems and result from a combination of surface templating with disassembly of the 3DOM structure (Figure 6). 3DOM materials consist of a 3D array of tetrahedra and octahedra (two tetrahedra for every octahedron) with concave faces. These polygonal particles are interconnected by "necks" at their vertices. Breaking or severing these necks via mechanical, chemical, or thermal means results in disassembly of the structure, yielding a bimodal distribution of nanoparticles with the original structure of the two types of nodes.[39,40]

When the organic content of the precursor is increased to many times the concentration of the metal ion, the organic components crowd out existing cations within the void spaces between spheres. Additionally, many polyester molecules are being formed that are not complexed to cations; these polymer molecules are charge-neutral. We propose that the metal-containing polyesters, being positively charged, have an affinity for the slightly negatively charged polymer spheres and thus aggregate at the surface of the PMMA spheres. A high degree of reactant imbalance aids in this process because the polymers

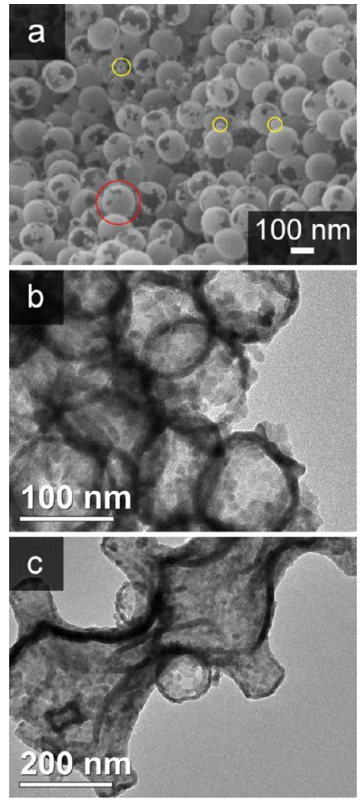

Figure 7. SEM and TEM images of Mn_3O_4 411 using a CCT template with 362 nm PMMA spheres. (a) SEM image highlighting the bimodal distribution of spheres. Red circles indicate large spheres, and yellow circles indicate small ones. (b) TEM image showing the hollow nature of the spheres. (c) TEM image showing a section of the sample with surface replication of the octahedral hole morphology without substantial densification. Samples were gelled at 90 °C for 24 h.

may remain small enough to diffuse throughout the CCT. During calcination, the space-filling organic material is removed, leaving only a thin shell of metal oxide. This process, leading to the formation of a hollow 3DOM structure, is known as surface templating.

dx.doi.org/10.1021/ic5023856 | Inorg. Chem. 2015, 54, 993−1002

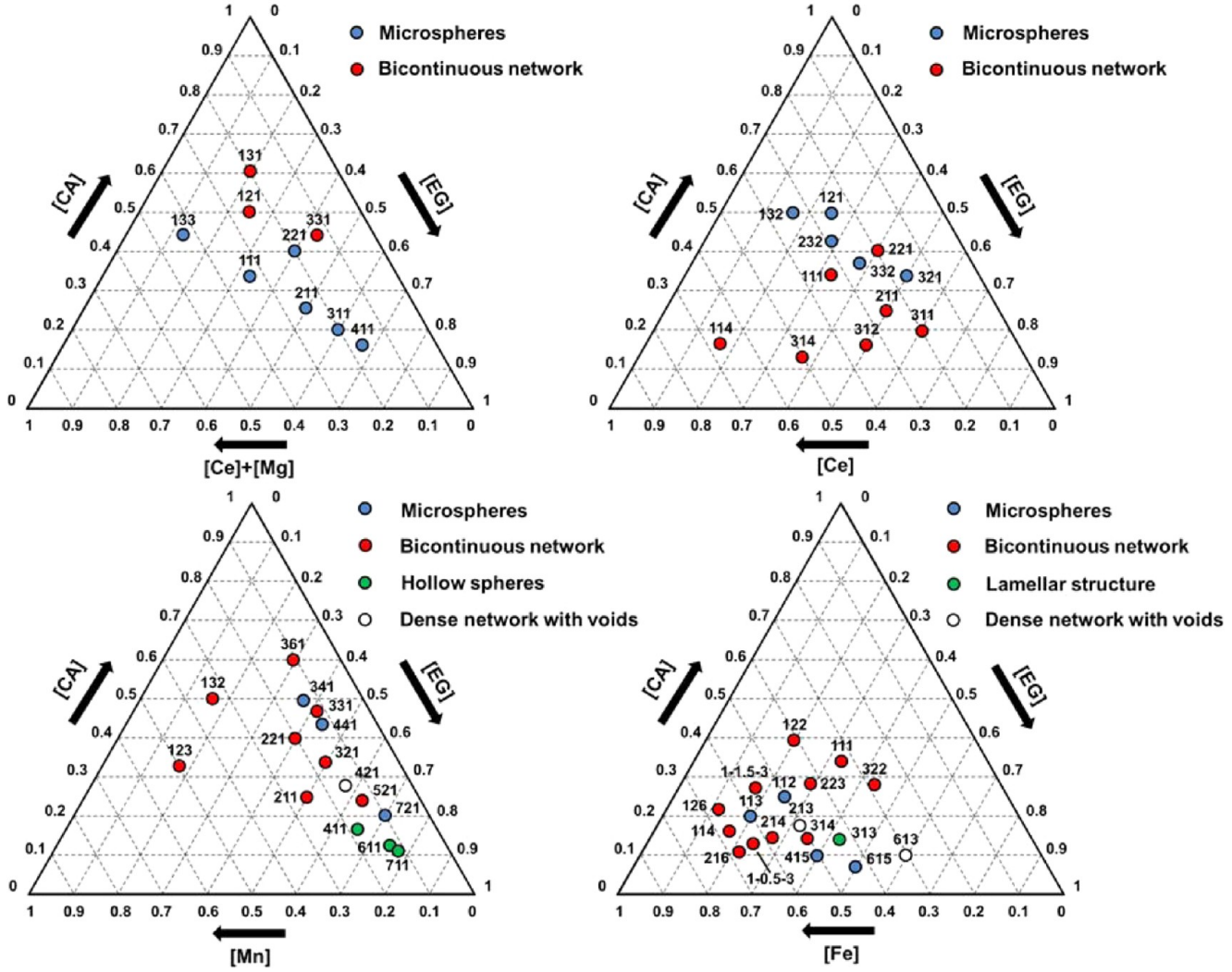

Figure 8. Quasi-phase diagrams generated from multiple precursor compositions and observations of the morphology in those samples for several metal oxides: $Ce_{0.5}Mg_{0.5}O_{1.5}$, CeO_2, Mn_3O_4, and Fe_2O_3.

Because of the very thin walls (<20 nm) and moderate calcination temperature (450 °C), the hollow Mn_3O_4 tetrahedra and octahedra undergo densification processes that minimize the surface energy of the particles, first severing the necks, then removing the concave nature of the original particles, and converting them to spherical shells. However, this process does not affect the low size dispersity and bimodal distribution of the resulting particles. The holes and gaps within the shells result from grain growth (solid-state diffusion) during calcination, in which some Mn_3O_4 nanocrystals increase in size through Ostwald ripening. In essence, the thickness of the shells increases, but at the expense of surface coverage. Transmission electron microscopy (TEM) of the particles reveals that they are indeed hollow (Figure 7b). In fact, in some rare areas of the sample, hollow octahedra that have not completed the surface minimization process can be observed (Figure 7c).

Construction of Partial Quasi-Phase Diagrams. A large number of compositions were produced and analyzed during the course of this investigation (see the SI). Categorizing the types of morphologies obtained for each synthesis and plotting the points versus EG, CA, and M^{q+} molar ratios allow for the construction of ternary quasi-phase diagrams for the metal oxides explored (Figures 8 and S5–S9 in the SI). As demonstrated above, K_f of the metal determines the position of the "microsphere" phase along the M^{q+} axis; the manganese-based materials tend to form microspheres with lower concentrations of metal relative to CA, and the iron-based materials tend to form microspheres at high concentrations of metal relative to CA. Slight deviations from compositions in the microsphere quasi-phase space tend to produce bicontinuous networks in all systems; this is particularly noticeable in Fe_2O_3 and Mn_3O_4, where the microsphere quasi-phase space is small and surrounded by bicontinuous network compositions. Additionally, with the exception of the mixed oxide $Ce_{0.5}Mg_{0.5}O_{1.5}$, the bicontinuous network phase is generally located toward the center of the diagram. The "hollow spheres" observed in the manganese system are observed only at high concentrations of EG and only with the smaller (362 nm) templating spheres.

Still, some questions remain. It is not apparent what controls the relative size of the phases for different metal ions; i.e., why is the range of EG/CA/M^{q+} ratios leading to microspheres for $Ce_{0.5}Mg_{0.5}O_{1.5}$ and CeO_2 different from that for Fe_2O_3 and Mn_3O_4? The quasi-phase space corresponding to particular microstructures may not be continuous, as in the Fe_2O_3

dx.doi.org/10.1021/ic5023856 | Inorg. Chem. 2015, 54, 993−1002

diagram, where compositions like 112 and 113 are separated from 415 and 615 with bicontinuous network samples in between. The origin of microstructures like Fe_2O_3 313 (Figure S8 in the SI) with partially separated lamellae (sheets) of 3DOM material are not well-understood. Finally, the effect of the binding mode (i.e., how many CA molecules per cation are involved in chelation) and the molecular structure of the complex on the molecular weight has not been investigated, and this relationship is not entirely clear. Further investigation of this method, particularly of the dynamics of gelation and the molecular weight of the metal-laced polyester under differing conditions, could yield still greater degrees of control over the microstructure in templated systems.

CONCLUSIONS

The parameters that control the microstructural variation of CeO_2 and $Ce_{0.5}Mg_{0.5}O_{1.5}$ through PIPS of precursors in templated Pechini-based syntheses were investigated. A variety of influencing factors were identified, including temperature, reagent concentration, number of functional groups in the complexing agent, counterion concentration, counterion identity, K_f of the CA−metal complex, and size of the templating polymer spheres. The common thread connecting these factors was that each of them affects the degree of polymerization during polyesterification, either through reaction kinetics, reagent imbalance, or confinement in the CCT. On the basis of SEM analyses of samples prepared under different conditions, a "continuum" of morphologies was proposed in which an increasing degree of polymerization results in morphological shifts, progressing along the following trend: full-volume 3DOM materials to 3DOM bicontinuous networks with high void fractions to 3DOM microspheres to 3DOM bicontinuous networks with high solid fractions and again to full-volume 3DOM materials. This proposed continuum was then applied to guide the synthesis of two model systems, Mn_3O_4 and Fe_2O_3, to test the continuum model, and to evaluate the ability to generalize this methodology. Many compositions were synthesized to construct ternary quasi-phase diagrams (EG vs CA vs TMI) for these systems, detailing the regions of particular microstructural regimes. Using the microsphere morphology as a test case, it was found that replacing the cation with manganese caused the quasi-phase space for microstructural variation to shift to high CA/M^{q+} ratios, whereas iron shifted that quasi-phase space to low CA/M^{q+} ratios. The average diameters for 3DOM microspheres formed by this method were in the range of 0.8−3.3 μm for $Ce_{0.5}Mg_{0.5}O_{1.5}$, 0.8−2.0 μm for CeO_2, 1.0−1.6 μm for Mn_3O_4, and 0.5−1.6 μm for Fe_2O_3 when 489 nm PMMA spheres were used in the CCT. The observations and insights gained from this work indicate the feasibility of generalizing PIPS-based microstructural control to other water-soluble and acid-stable cations.

ASSOCIATED CONTENT

Supporting Information

Materials and characterization methods, detailed calculation of O_h and T_d hole sizes, morphological description, compositional information, and SEM images for 54 samples synthesized over the course of this work, chemical structures for monomers used in polyesterification, SEM images of template spheres as-synthesized and exposed to EG or glycerin, and powder XRD patterns of representative Mn_3O_4 and Fe_2O_3/Fe_3O_4 samples. This material is available free of charge via the Internet at http://pubs.acs.org.

AUTHOR INFORMATION

Corresponding Author

*E-mail: a-stein@umn.edu. Tel: +1-612-624-1802. Fax: +1-612-626-7541.

Notes

The authors declare no competing financial interest.

ACKNOWLEDGMENTS

This project was funded by the University of Minnesota Initiative for Renewable Energy and the Environment. Portions of this work were carried out in the University of Minnesota Characterization Facility, which receives partial support from the NSF through the MRSEC, ERC, MRI, and NNIN programs. S.G.R. was supported by a Doctoral Dissertation Fellowship from the University of Minnesota Graduate School. B.-L.S. and R.L. thank the University of Namur for an internship grant.

REFERENCES

(1) Wang, S.; Lu, Z.; Wang, D.; Li, C.; Chen, C.; Yin, Y. *J. Mater. Chem.* **2011**, *21*, 6365−6369.
(2) Parlett, C. M. A.; Wilson, K.; Lee, A. F. *Chem. Soc. Rev.* **2013**, *42*, 3876−3893.
(3) Twigg, M. V.; Richardson, J. T. *Ind. Eng. Chem. Res.* **2007**, *46*, 4166−4177.
(4) Sun, Z.; Sun, B.; Qiao, M.; Wei, J.; Yue, Q.; Wang, C.; Deng, Y.; Kaliaguine, S.; Zhao, D. *J. Am. Ceram. Soc.* **2012**, *134*, 17653−17660.
(5) Shao, Y.; Liu, J.; Wang, Y.; Lin, Y. *J. Mater. Chem.* **2009**, *19*, 46−59.
(6) Ruiz-Morales, J. C.; Canales-Vázquez, J.; Peña-Martínez, J.; Marrero-López, D.; Irvine, J. T. S.; Núñez, P. *J. Mater. Chem.* **2006**, *16*, 540−542.
(7) Brandon, N. P.; Brett, D. J. *Philos. Trans. R. Soc., A* **2006**, *364*, 147−159.
(8) Jacobson, A. J. *Chem. Mater.* **2010**, *22*, 660−674.
(9) Leofanti, G.; Padovan, M.; Tozzola, G.; Venturelli, B. *Catal. Today* **1998**, *41*, 207−219.
(10) Rudisill, S. G.; Venstrom, L. J.; Petkovich, N. D.; Quan, T.; Hein, N.; Boman, D. B.; Davidson, J. H.; Stein, A. *J. Phys. Chem. C* **2012**, *117*, 1692−1700.
(11) Nakanishi, K.; Tanaka, N. *Acc. Chem. Res.* **2007**, *40*, 863−873.
(12) Brinker, C. J.; Scherer, G. W. *Sol−gel science: the physics and chemistry of sol−gel processing*; Gulf Professional Publishing: Houston, TX, 1990.
(13) Kakihana, M. *J. Sol−Gel Sci. Technol.* **1996**, *6*, 7−55.
(14) Cividanes, L. S.; Campos, T. M.; Rodrigues, L. A.; Brunelli, D. D.; Thim, G. P. *J. Sol−Gel Sci. Technol.* **2010**, *55*, 111−125.
(15) Stein, A.; Wilson, B. E.; Rudisill, S. G. *Chem. Soc. Rev.* **2013**, *42*, 3721−3739.
(16) Titirici, M.-M.; Antonietti, M.; Thomas, A. *Chem. Mater.* **2006**, *18*, 3808−3812.
(17) Wan, Y.; Zhao, D. *Chem. Rev.* **2007**, *107*, 2821−2860.
(18) Petkovich, N. D.; Stein, A. Colloidal Crystal Templating Approaches to Materials with Hierarchical Porosity. In *Hierarchically Structured Porous Materials: From Nanoscience to Catalysis, Separation, Optics, Energy, and Life Science*; Su, B.-L., Sanchez, C., Yang, X.-Y., Eds.; Wiley-VCH Verlag GmbH & Co. KGaA: Weinheim, Germany, 2012; Vol. *1*, pp 55−129.
(19) Rauda, I. E.; Buonsanti, R.; Saldarriaga-Lopez, L. C.; Benjauthrit, K.; Schelhas, L. T.; Stefik, M.; Augustyn, V.; Ko, J.; Dunn, B.; Wiesner, U.; Milliron, D. J.; Tolbert, S. H. *ACS Nano* **2012**, *6*, 6386−6399.
(20) Fu, M.; Zhao, A.; He, D.; Wang, Y. *Chem. Mater.* **2014**, *26*, 3084−3088.

(21) Fu, M.; Cui, J.; Yang, M.; Jiang, R.; He, D.; Wang, Y. *Cryst. Res. Technol.* **2012**, *47*, 1249−1254.
(22) Li, C.; Qi, L. *Angew. Chem., Int. Ed.* **2008**, *47*, 2388−2393.
(23) Hetherington, N. B. J.; Kulak, A. N.; Kim, Y.-Y.; Noel, E. H.; Snoswell, D.; Butler, M.; Meldrum, F. C. *Adv. Funct. Mater.* **2011**, *21*, 948−954.
(24) Nakanishi, K.; Soga, N. *J. Am. Ceram. Soc.* **1991**, *74*, 2518−2530.
(25) Nakanishi, K. *J. Porous Mater.* **1997**, *4*, 67−112.
(26) Nakanishi, K.; Soga, N. *J. Non-Cryst. Solids* **1992**, *139*, 1−13.
(27) Nakanishi, K.; Soga, N. *J. Non-Cryst. Solids* **1992**, *139*, 14−24.
(28) Rudisill, S. G.; Hein, N. M.; Terzic, D.; Stein, A. *Chem. Mater.* **2013**, *25*, 745−753.
(29) Pechini, M. A method of preparing lead and alkaline earth titanates and niobates and coating method using the same to form a capacitor. U.S. Patent 3,330,697, July 11, 1967.
(30) Schroden, R. C.; Al-Daous, M.; Sokolov, S.; Melde, B. J.; Lytle, J. C.; Stein, A.; Carbajo, M. C.; Fernández, J. T.; Rodríguez, E. E. *J. Mater. Chem.* **2002**, *12*, 3261−3267.
(31) Odian, G. *Principles of Polymerization*, 3rd ed.; John Wiley & Sons, Inc.: Hoboken, NJ, 1991; pp 110−115.
(32) Hiemenz, P. C.; Lodge, T. P. *Polymer Chemistry*, 2nd ed.; CRC Press: Boca Raton, FL, 2007; p 54.
(33) Getsova, M.; Todorovsky, D.; Enchev, V.; Wawer, I. *Monatsh. Chem.* **2007**, *138*, 389−401.
(34) Martell, A. E.; Smith, R. M. *Critical Stability Constants: Inorganic Complexes*; Plenum Press: New York, 1989; Vol. *4*.
(35) Zakhidov, A. A.; Baughman, R. H.; Iqbal, Z.; Cui, C.; Khayrullin, I.; Dantas, S. O.; Marti, J.; Ralchenko, V. G. *Science* **1998**, *282*, 897−901.
(36) Stein, A.; Rudisill, S. G.; Petkovich, N. D. *Chem. Mater.* **2013**, *26*, 259−276.
(37) Dong, W.; Bongard, H. J.; Marlow, F. *Chem. Mater.* **2003**, *15*, 568−574.
(38) Dong, W.; Marlow, F. *Microporous Mesoporous Mater.* **2007**, *99*, 236−243.
(39) Li, F.; Wang, Z.; Stein, A. *Angew. Chem., Int. Ed.* **2007**, *46*, 1885−1888.
(40) Stein, A.; Li, F.; Wang, Z. *J. Mater. Chem.* **2009**, *19*, 2102−2106.